energies

MDPI

Article

Modified Current Sensorless Incremental Conductance Algorithm for Photovoltaic Systems

Víctor Ferreira Gruner [1], Jefferson William Zanotti [2], Walbermark Marques Santos [3], Thiago Antonio Pereira [1], Lenon Schmitz [1], Denizar Cruz Martins [1] and Roberto Francisco Coelho [1,*]

[1] Department of Electrical and Electronics Engineering, Federal University of Santa Catarina, Florianopolis 88040-900, Brazil; victor.gruner@posgrad.ufsc.br (V.F.G.); thiagopereira.eel@gmail.com (T.A.P.); lenonsch@gmail.com (L.S.); denizar.martins@gmail.com (D.C.M.)
[2] Department of Electrical Engineering, Federal Institute of Santa Catarina, Jaragua do Sul 89254-430, Brazil; jefferson.zanotti@ifsc.edu.br
[3] Department of Electrical Engineering, Federal University of Espirito Santo, Vitoria 29075-910, Brazil; walbermark.santos@ufes.br
* Correspondence: roberto.inep@gmail.com; Tel.: +55-48-3721-7464

Abstract: This paper proposes a novel maximum power point tracking algorithm applied to photovoltaic systems. The proposed method uses the derivative of power versus voltage to define the tracking path and has the advantage of requiring only a voltage sensor to be implemented. The absence of the current sensor and the auxiliary circuitry employed for conditioning the current signal imply cost reduction, configuring the main contribution of the proposed method, whose performance is kept close to the classical incremental conductance method, even with the reduced number of components. A DC-DC zeta converter is introduced in the content of this work as an interface between a photovoltaic array and a resistive load. The paper describes the operating principle and presents the mathematical formulation related to the proposed algorithm. Interesting simulation and experimental results are presented to validate the theory by comparing the proposed method with its traditional version under several scenarios of solar irradiance and temperature.

Keywords: current sensorless tracking algorithm; incremental conductance; maximum power point tracker

Citation: Gruner, V.F.; Zanotti, J.W.; Santos, W.M.; Pereira, T.A.; Schmitz, L.; Martins, D.C.; Coelho, R.F. Modified Current Sensorless Incremental Conductance Algorithm for Photovoltaic Systems. *Energies* **2023**, *16*, 790. https://doi.org/10.3390/en16020790

Academic Editor: Luis Hernández-Callejo

Received: 14 December 2022
Revised: 3 January 2023
Accepted: 4 January 2023
Published: 10 January 2023

1. Introduction

Photovoltaic (PV) generation has become a viable alternative for sustainable energy generation. Besides the advantages of reduced maintenance, modularity, and low levels of noise and pollutants emissions, the cost of PV energy is decreasing year after year [1,2]. Nevertheless, photovoltaic modules still present low peak conversion efficiency: while in the laboratory multijunction solar cells have shown maximum efficiencies of around 47%, the weighted average efficiencies of crystalline silicon-based modules are ranged between 16% and 22% in commercial applications [2]. Additionally, the mentioned efficiency is only accomplished when the PV modules operate at the standard test conditions (STC), which makes the real efficiency still lower than the value specified in datasheets.

In practice, the output powers of PV modules are strongly affected by the environmental conditions, such as the incoming solar irradiance (S) and the operating temperature (T). For each combination of S and T, there is a unique operating point in which the generated power reaches its maximum value. This operating point is named by Maximum Power Point (MPP) [3–36]. Since in real operation it is unfeasible to control the environmental conditions, the maximum power point oscillates following the solar irradiance and temperature changes.

A PV module is said to be operating at the MPP when the product of its voltage V_{pv} by its current I_{pv} reaches the maximum value. However, since this desired operating point

moves over time, it needs to be actively tracked. Typically, dc-dc converters controlled by tracking algorithms are employed for this finality. These converters are named by maximum power point trackers (MPPT) [3–36]. In the literature, there are several proposals of tracking algorithms. The constant duty cycle and constant voltage methods are featured by simple practical realization. However, they present a poor tracking factor [3–9].

Some techniques based on Fuzzy Logic [3–9] and neural network [15,16] present satisfactory tracking factors but require high computational cost and complex realization. Other methods such as the temperature-based method and the Beta method have high tracking factors, but they are dependent on parameters of the module, which can cause tracking mismatch with aging [17,18].

The recurrent perturb and observe (P&O) method is usually cited as a suitable solution because it presents a good cost-benefit between tracking factor and simple realization [19–22]. However, there are some drawbacks inherent to this method: firstly, it cannot simultaneously comply fast tracking and low steady state oscillations around the MPP and, secondly, abrupt changes in the solar irradiance often disturb the tracking path, implying a reduction in the tracking factor, mainly in partially cloudy days [3–9,19–22].

Conversely, the incremental conductance (IncCond) method has become the most effective among the conventional techniques previously cited, since it allows obtaining a satisfactory tracking factor and a simple implementation, in addition to complying with fast tracking and low steady-state oscillations around the MPP [23–28]. This method is based on the P-V curve, where the derivative of the power with respect to the voltage (dP_{pv}/d_{Vp}) is positive to the left of the MPP, negative to the right of the MPP, and exactly zero on it.

It is worth mentioning that in recent years, several modified versions of the classical IncCond algorithm have also been introduced in the literature to further improve its performance [23–28]. The modified version proposed in [24] allows the full elimination of division calculations, thus simplifying the structure of the algorithm. This proposal reduces real-time processing, which allows the algorithm to be implemented by low-cost microcontrollers. Furthermore, in [25] a hybrid maximum power point tracking algorithm is obtained by combining the linear open-circuit voltage method and the variable step-size incremental conductance method. The authors emphasize that their proposal can harvest the maximum power from PV modules with a better performance than the individual methods. Similarly, [26] proposes a modified algorithm that combines the classical IncCond with the constant voltage method to estimate the MPP voltage. This approach limits the search space to increase the algorithm performance under transient conditions.

Although the IncCond method and all its variations present a proper static-dynamic performance, they require the usage of two sensors, to measure the voltage and the current across the PV generator [3–5]. Therefore, to derive a more reliable and low cost MPPT algorithm, in this paper, a new version of the classical IncCond algorithm is proposed, in which the current sensor and its conditioning circuitry are suppressed, and the derivative of the power with respect to the voltage is calculated only from reading the output voltage of the PV generator.

The remaining of this paper is organized as follows: in Section 2 a single-diode five-parameters PV array modelling is presented. This model is applied to validate the proposed tracking method in simulation platforms. In Section 3 the proposed tracking algorithm is formulated, and in Section 4 its performance is evaluated by simulation and experimentation under different scenarios of solar irradiance and temperature. In Section 5 a comparison analysis and discussions are addressed. Finally, the main findings conclude the paper in Section 6.

2. Five-Parameters One-Diode Model

The knowledge of the I-V and P-V curves plays an important role in the optimal design of MPPT systems, as it allows verifying the tracking path after changes in solar irradiance and temperature. Nevertheless, information contained in the manufacturer's datasheets

generally targets the PV electrical variables only for two operating points: standard test conditions (STC) and nominal operating temperature cell (NOTC). Therefore, for any other climate condition, the I-V and P-V curves need to be experimentally plotted or extrapolated from numerical models [35–41]. For this purpose, the five-parameters one-diode model shown in Figure 1 is the electrical model most cited in the technical literature to simulate photovoltaic generators [35–42].

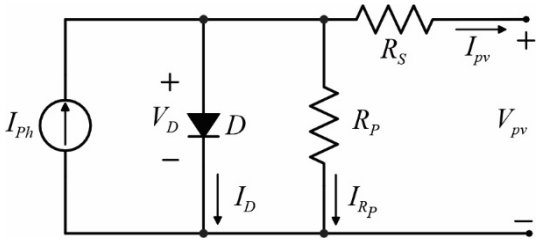

Figure 1. Five-parameters one-diode model.

In this model, I_{ph} represents the current generated by the photon-electron interaction, R_S (series resistance) the losses in the electrical contacts, R_P (shunt resistance) the losses generated by the leakage current, and D (diode) confers the nonlinear behaviour of the real PV module to the circuit. The variables V_{pv} and I_{pv} address the output voltage and current, related by:

$$I_{pv} = \frac{S}{S_{STC}} I_{ph}[1 + (T - T_{STC})\alpha] - I_S \left(\frac{T}{T_{STC}}\right)^3 \left[e^{\frac{q(V_{pv}+R_S I_{pv})}{AkT}} - 1\right] e^{\frac{qE_G}{Ak}\left(\frac{1}{T_{STC}} - \frac{1}{T}\right)} - \left[\frac{R_S I_{pv} + V_{pv}}{R_P}\right]. \quad (1)$$

To simplify the understanding of (1), Table 1 summarizes the meaning of each variable and reveals that the solution of (1) is only possible from the prior determination of five unknown variables: A, I_S, I_{ph}, R_S, and R_P. However, to obtain these five parameters, it is necessary to find five equations relating them. As a first step to obtain these equations, it can be assumed that the photovoltaic generator operates at the STC by setting $S = S_{STC}$ and $T = T_{STC}$. Thus, (1) can be simplified and rewritten as:

$$I_{pv} = I_{ph} - I_S \left[e^{\frac{q(R_S I_{pv}+V_{pv})}{AkT_{STC}}} - 1\right] - \frac{R_S I_{pv} + V_{pv}}{R_P}. \quad (2)$$

Table 1. Description of the variables from (1).

Parameter	Description	Value
Input and output variables	Incoming irradiance	S [W/m^2]
	Junction temperature	T [K]
	PV output current	I_{pv} [A]
	PV output voltage	V_{pv} [V]
Datasheet variables	Reference irradiance	S_{STC} = 1000 W/m^2
	Reference temperature	T_{STC} = 298 K
	Temperature coefficient of I_{SC}	α [%/K]
Constants	Elementary charge	$q = 1.602 \times 10^{-19}$ C
	Boltzmann Constant	$k = 1.38 \times 10^{-23}$ J/K
	Band gap energy	E_g = 1.12 eV
Variables to be determined	Ideality factor	A
	Photogenerated current under the reference conditions	I_{ph} [A]
	Reverse saturation current under the reference conditions	I_s [A]
	Series resistance	R_S [Ω]
	Parallel resistance	R_P [Ω]

As manufacturers specify three operating points at the STC in their datasheets, three of the five required equations can be directly determined. These equations describe the operation of the PV generator at the open-circuit voltage (V_{OC}, 0), short- circuit current (0, I_{SC}), and maximum power point (V_{MP}, I_{MP}). To determine the remaining two equations, one can consider that the derivative of the power with respect to the voltage (dP_{pv}/dV_{pv}) at the maximum power point is zero, and that the derivative of the current with respect to the voltage (dI_{pv}/dV_{pv}) at the short circuit point is equal to $-1/R_p$. From these assumptions, it is obtained the system of equations described in (3).

Once the five parameters have been determined by solving the system of equations presented in (3), they can be replaced into (1) and the theoretical I-V and P-V curves may be plotted for any solar irradiance and temperature conditions. The adoption of this procedure allows determining the five parameters related to the KC200GT photovoltaic module, as shown in Table 2. The respective I-V and P-V curves are depicted in Figure 2.

$$\begin{cases} I_{SC} = I_{ph} - I_S\left(e^{\frac{q(R_S I_{SC})}{AkT_{STC}}} - 1\right) - \frac{R_S I_{SC}}{R_P} \\ 0 = I_{ph} - I_S\left(e^{\frac{qV_{OC}}{AkT_{STC}}} - 1\right) - \frac{V_{OC}}{R_P} \\ I_{MP} = I_{ph} - I_S\left(e^{\frac{q(R_S I_{SC}+V_{MP})}{AkT_{STC}}} - 1\right) - \frac{R_S I_{MP}+V_{MP}}{R_P} \\ R_S + \frac{qI_S R_P(R_S-R_P)}{AkT_{STC}} e^{\frac{qI_{SC}}{AkT_{STC}}} = 0 \\ I_{ph} - \frac{2V_{MP}}{R_P} - I_S\left(1 + \frac{q(V_{MP}-R_S I_{MP})}{AkT_{STC}}\right) e^{\frac{q(R_S I_{MP}+V_{MP})}{AkT_{STC}}} + I_S = 0 \end{cases} \quad (3)$$

Table 2. One-diode model parameters related to the PV module KC200GT.

Parameters	KC200GT
I_{ph}	8.2119 A
I_s	171.07 nA
A	1.3411
R_S	0.2172 Ω
R_P	951.927 Ω

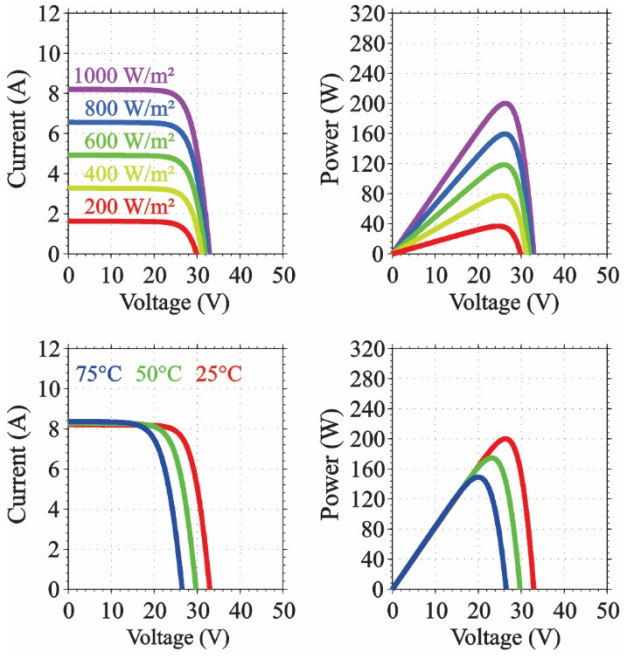

Figure 2. KC200GT I-V and P-V curves obtained from the one-diode model.

3. The Proposed Tracking Algorithm

In a typical configuration, a MPPT system is composed of a PV generator, a DC-DC converter, and a load, as shown in Figure 3. Considering that the dc-dc converter operates at continuous-conduction mode (CCM) and feeds a resistive load R_o, it is possible to express the PV voltage V_{pv} and current I_{pv} as a function of the static gain G, the output voltage V_o, and the output current I_o:

$$V_{pv} = \frac{V_o}{G}, \tag{4}$$

$$I_{pv} = GI_o. \tag{5}$$

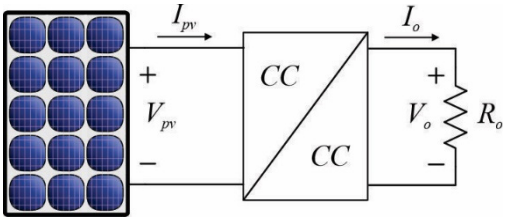

Figure 3. DC-DC converter applied as MPPT.

Thus, dividing (4) by (5) one can express the ratio between the V_{pv} and I_{pv}, which can be understood as the effective input resistance R_i seen by the PV generator, as:

$$R_i = \frac{V_{pv}}{I_{pv}} = \frac{1}{G^2}\frac{V_o}{I_o} = \frac{R_o}{G^2}. \tag{6}$$

This result allows simplifying Figure 3 as shown in Figure 4 and thus expressing the power delivered by the PV generator as:

$$P_{pv} = \frac{{V_{pv}}^2}{R_{pv}} = \frac{{V_{pv}}^2 G^2}{R_o}. \tag{7}$$

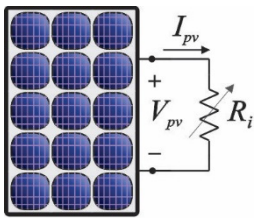

Figure 4. Simplified equivalent circuit of a DC-DC converter feeding a resistive load.

As in the traditional IncCond method, the derivative of P_{pv} with respect to V_{pv} needs to be determined. Therefore, using (7) one can write:

$$\frac{dP_{pv}}{dV_{pv}} = \frac{2V_{pv}G^2}{R_o} + \frac{{V_{pv}}^2}{R_o}\frac{dG^2}{dV_{pv}}. \tag{8}$$

In practice, MPPT algorithms are typically implemented in digital platforms (microcontroller or DSP, for example), so that the derivative terms may be approximated by small variations that occur between the current (k) and previous ($k-1$) sampling periods. Therefore:

$$\frac{\Delta P_{pv}}{\Delta V_{pv}} = \frac{V_{pv}G^2}{R_o}\left[2 + \frac{V_{pv}}{\Delta V_{pv}}\left(\frac{\Delta G}{G}\right)^2\right], \tag{9}$$

where:

$$\begin{cases} \Delta P_{pv} = P_{pv(k)} - P_{pv(k-1)} \\ \Delta V_{pv} = V_{pv(k)} - V_{pv(k-1)} \\ \Delta G = G_{(k)} - G_{(k-1)} \end{cases}. \quad (10)$$

The search for the MPP ends when $\Delta P_{pv}/\Delta V_{pv}$ becomes null. Until this condition is true, the result of $\Delta P_{pv}/\Delta V_{pv}$ may be evaluated to determine the tracking path, according to the following rule:

$$\begin{cases} \frac{\Delta P_{pv}}{\Delta V_{pv}} = 0 \rightarrow \frac{V_{pv}}{\Delta V_{pv}}\left(\frac{\Delta G}{G}\right)^2 = -2 \rightarrow \text{at MPP} \\ \frac{\Delta P_{pv}}{\Delta V_{pv}} > 0 \rightarrow \frac{V_{pv}}{\Delta V_{pv}}\left(\frac{\Delta G}{G}\right)^2 > -2 \rightarrow \text{left of MPP} \\ \frac{\Delta P_{pv}}{\Delta V_{pv}} < 0 \rightarrow \frac{V_{pv}}{\Delta V_{pv}}\left(\frac{\Delta G}{G}\right)^2 < -2 \rightarrow \text{right of MPP} \end{cases}. \quad (11)$$

As noticed, Equation (11) reveals that $\Delta P_{pv}/\Delta V_{pv}$ depends on V_{pv} and G at the instants (k) and $(k-1)$. The value of V_{pv} is measured in each sampling period and the value of G is calculated from the DC-DC converter operating duty cycle D. Table 3 summarizes the relation between G and D for the basic non-isolated DC-DC converters at CCM.

Table 3. Input resistance of the main non-isolated DC-DC converters.

Converters	G	R_i
Buck	D	$\frac{R_o}{D^2}$
Boost	$\frac{1}{1-D}$	$R_o(1-D)^2$
Buck-Boost, Ćuk, SEPIC and Zeta	$\frac{D}{1-D}$	$R_o\left(\frac{1-D}{D}\right)^2$

To implement the proposed tracking method, only one voltage sensor is required to measure the voltage of the PV generator, as illustrated in Figure 5. It can be considered the great advantage over the traditional incremental conductance method. The current sensor that is avoided would cost from cents to tens of dollars depending on technology used, which may range from shunt resistors to hall effect current sensors, in addition to costs related to the auxiliary circuitry employed for signal conditioning. Moreover, the need for fewer analog inputs may eventually be advantageous, since it is a limiting factor in choosing the microcontroller.

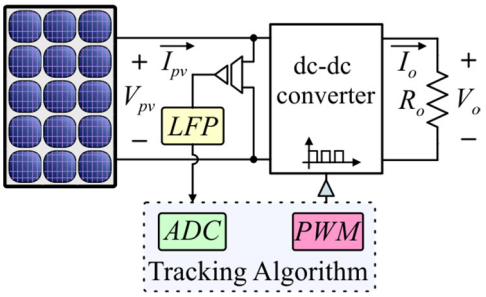

Figure 5. MPPT system for evaluating the proposed tracking algorithm.

According to the flowchart described in Figure 6, the algorithm is initialized by the reading of $V_{pv(k)}$ and through the calculation of $G_{(k)}$ considering the current value of the duty cycle $D_{(k)}$, as described in Table 3. Because the values of $V_{pv(k-1)}$ and $G_{(k-1)}$ were

previously buffered, Equation (11) can be evaluated to determine whether the duty cycle should be increased or decreased by a fixed step size ΔD, accordingly with:

$$\begin{cases} D_{(k)} = D_{(k-1)} \rightarrow \text{at MPP} \\ D_{(k)} = D_{(k-1)} - \Delta D \rightarrow \text{left of MPP} \\ D_{(k)} = D_{(k-1)} + \Delta D \rightarrow \text{right of MPP} \end{cases} . \quad (12)$$

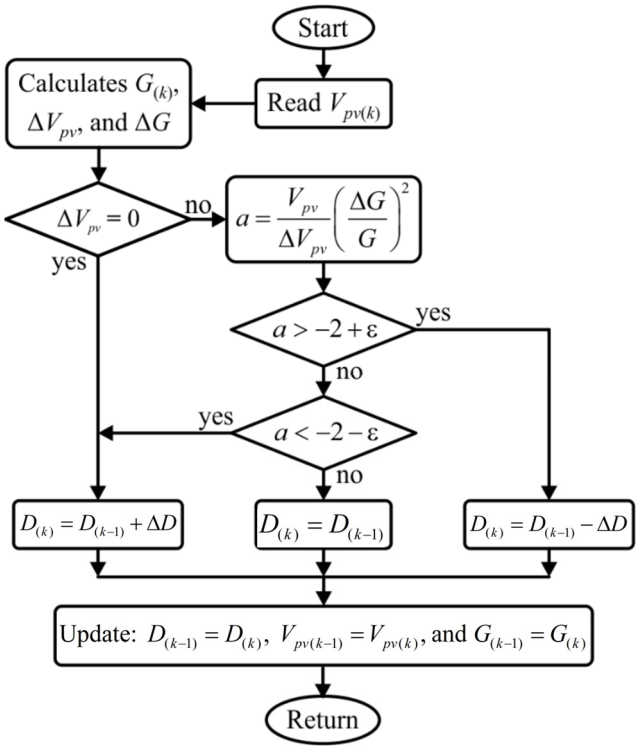

Figure 6. Flowchart of the proposed tracking algorithm.

It is important to highlight that during the first iteration the buffered quantities may be set to be null, except for $D_{(k)}$, which is initialized with a non-null value to avoid a division by zero during the calculation of $G_{(k)}$. For the same reason, an alternative routine is implemented to bypass the term $\Delta P_{pv}/\Delta V_{pv}$ when $\Delta V_{pv} = 0$. If this condition is true, the duty cycle $D_{(k-1)}$ is incremented to change the PV output voltage to another operating point from which the algorithm continues. Nevertheless, in discrete-time realization, the condition $\Delta P_{pv}/\Delta V_{pv} = 0$ may never be matched. Thus, the system is considered as operating at the MPP if $|\Delta P_{pv}/\Delta V_{pv}| < \varepsilon$, in which ε is a small positive number defined as a function of the resolution of the microcontroller.

4. Performance Evaluation under Irradiance and Temperature Changes

As previously mentioned, DC-DC converters have been extensively applied as MPPT and they must be able to track the MPP under any climate conditions. For this purpose, the operating point of the PV module must be varied from open circuit to short circuit; in other words, the DC-DC converter needs to emulate input resistances in the range from zero to infinite. This condition restricts the selection of the basic DC-DC converters to the Buck-Boost, Ćuk, SEPIC or Zeta topologies [10–14]. Among these four topologies, the Zeta converter is herein employed as a power stage.

Figure 7 illustrates a simplified block diagram of the proposed system, whose operation is described as follows: a microcontroller receives the voltage (V_{pv}) of the PV module and generates the duty cycle D to be applied to the Zeta converter that emulates an input resistance R_i to impose the operating point of the PV module at the MPP. The adopted

sampling frequency (f_{samp}) is 10 Hz. Thus, the algorithm defines a new duty cycle value every 0.1 s.

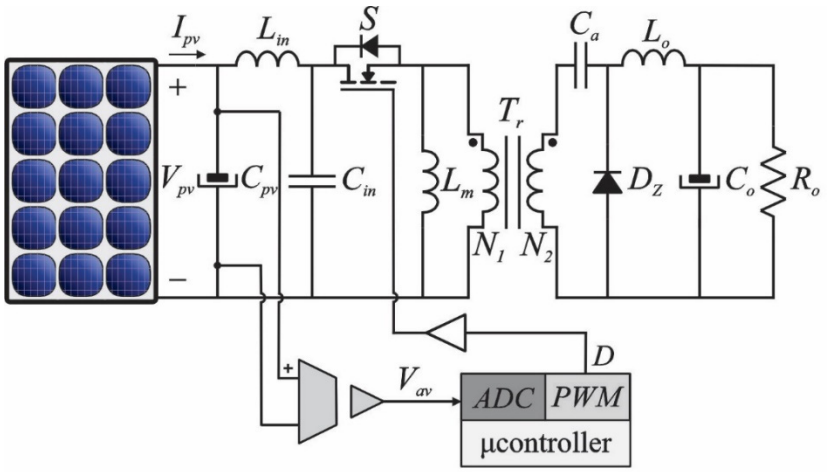

Figure 7. Block diagram of the proposed tracking system employing a Zeta converter as power stage.

Table 4 shows the main parameters related to the laboratory prototype illustrated in Figure 8. The proposed MPPT method was experimentally evaluated to validate its proper operation. The PV array is emulated by the Magna Power TSA500-40 emulator, considering a string of five series-connected KC200GT modules operating at the NOCT (800 W/m^2 and 47 °C). In this condition, the theoretical values of voltage and current at the maximum power point are respectively 116 V and 6.13 A, as listed in Table 5.

Table 4. Zeta Converters Parameters.

Parameters	Values and Components
Maximum input voltage (V_{pv})	180 V
Output voltage (V_o)	180 V
Efficiency (η)	90%
Maximum input power (P_{in})	1400 W
Switching frequency (f_s)	50 kHz
Magnetizing inductance (L_m)	0.99 mH
Output inductor filter (L_o)	4.99 mH
Input inductor filter (L_{in})	0.2 mH
Input capacitor filter (C_{in})	5.0 µF
Input bus capacitor (C_{pv})	180 µF
Coupling capacitor (C_a)	20 µF
Output capacitor filter (C_o)	1.0 µF
MOSFET (S)	IPW60R070C6-650 V/34 A
Diode (D_z)	IXYSDSEI 60-1200 V/52 A
Microcontroller	PIC18F1320—8 bits

Table 5. Electrical specifications of the PV array @ S = 800 W/m^2 and T = 47 °C (NOTC).

Parameters	Values
Maximum power point P_{mp}	710 W
Maximum power voltage V_{mp}	116 V
Maximum power current I_{mp}	6.13 A
Open circuit voltage V_{oc}	149.5 V
Short circuit current I_{sc}	6.62 A

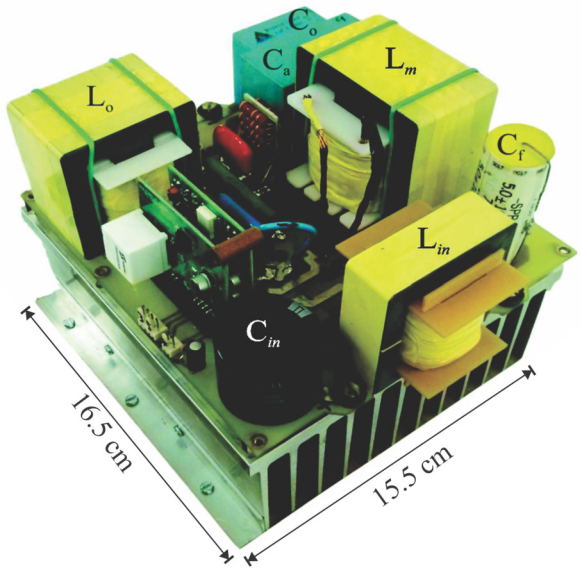

Figure 8. Zeta converter prototype.

The voltage sensor is performed by a resistive divider and the algorithm is embedded in the 8-bits PIC18F1320 microcontroller. The duty cycle step size is set to $\Delta D = 0.05$ and it is considered $\varepsilon = 0.02$, which is higher than the pulse width modulation (PWM) resolution. It is worth mentioning that the adjustment of the step size is a major concern in any conventional hill climb algorithm, such as the IncCond and the perturb and observe (P&O), since it defines the tradeoff between steady-state oscillation and tracking speed. The implementation of a variable step size algorithm, as in [23], is possible and would allow the usage of a large step size when the operating point is far from the MPP (high dP/dV) and a reduced step size as the operating point finds the vicinity of the MPP (low dP/dV), decreasing the steady-state oscillation while keeping a fast-tracking speed.

4.1. Performance Verification under Irradiance Changes and Constant Temperature and Load

This test was performed by maintaining the temperature and the load resistance constant at 47 °C and 94.4 Ω, respectively, and applying irradiance steps of 200 W/m^2 on every 20 s. Figure 9a,b show the evolution of the PV array output power during the irradiance changes, while Figure 9c,d show the comparison between the expected theoretical value and the tracked maximum power point for both, experimental and simulation scenarios. It is worth mentioning that the expected theoretical values were obtained from the one-diode model, which can slightly diverge from the I-V curve generated by the Magna Power TSA500-40 emulator.

4.2. Performance Verification under Temperature Changes and Constant Irradiance and Load

This test was performed considering two scenarios. Initially, a step of 10 °C was applied to the temperature, as depicted in Figure 10a. Furthermore, since the voltage and the power generated by PV modules are strongly affected by temperature variations, in Figure 10b, an additional step of 30 °C was applied to highlight the impact of temperature in the tracking dynamics of the proposed algorithm. As can be verified from the simulation and experimental results represented in Figure 10c,d, after the transient response, the tracked power approximately matches the expected theoretical value.

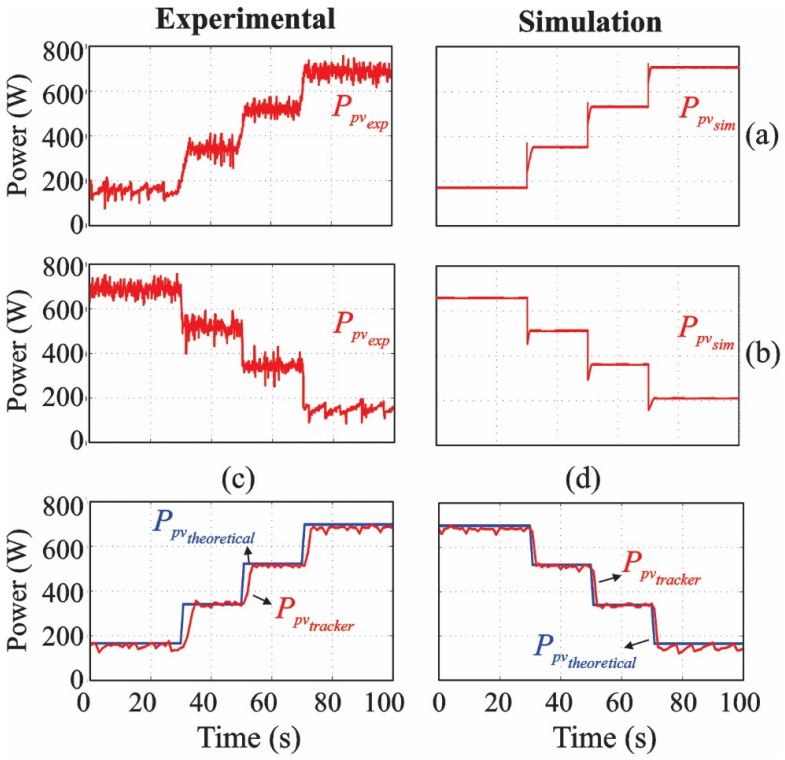

Figure 9. PV array output power under (**a**) increasing and (**b**) decreasing of irradiance with T = 47 °C. Comparison between the theoretical and the tracked maximum power point (**c**,**d**).

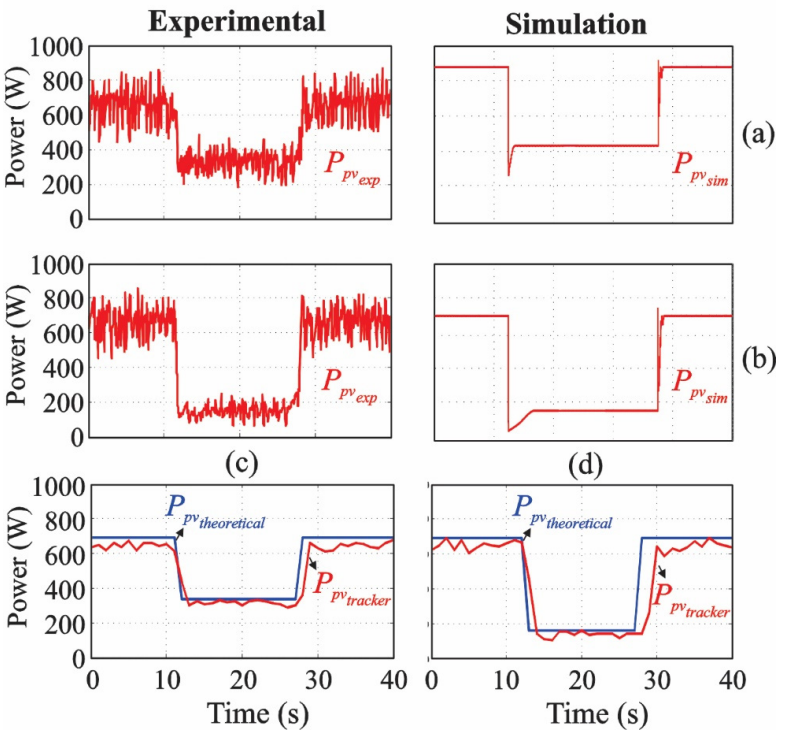

Figure 10. PV array output power considering temperature changes of (**a**) 10 °C and (**b**) 30 °C with S = 800 W/m^2. Comparison between the theoretical and the tracked maximum power point during the temperature changes (**c**,**d**).

5. Comparison Analysis and Discussion

In the technical literature, tracking algorithms are usually classified as indirect, direct, and based on artificial intelligence [42]. Indirect algorithms make use of information previously stored in databases, as the voltage, current, and power values under several different climate conditions. The microcontroller that executes the algorithm receives the acquisitions of the system variables and compares them with those stored to define the value of voltage or current to be used as a tracking reference. These methods require the use of sensors applied for reading solar irradiance and temperature. Therefore, they are not economically justified in small and medium size applications.

On the other hand, the direct algorithms do not use information stored in a database, making use of measurements of system variables to verify the location of the operating point in relation to the MPP and acting so that they converge with each other. Generally, these algorithms present oscillations, as the tracking direction is determined in real time, based on the measurements performed at each iteration.

There are even some algorithms based on the use of artificial intelligence. Normally, these algorithms are similar to the direct ones, but supported by neural networks and fuzzy logic techniques, a fact that results in better performance, especially in conditions of partial shading. However, because they are more complex, they require more computational capacity to be carried out.

To demonstrate the proposed method effectiveness, it was firstly compared with the conventional Incremental Conductance algorithm under irradiance and temperature changes. The first tests were performed by maintaining the temperature and the load resistance constant at 47 °C and 94.4 Ω, respectively. The evolution of the PV array output power was acquired for different levels of irradiance, by applying steps of 200 W/m^2 on every 20 s from 400 W/m^2 to 1000 W/m^2 and vice-versa.

Figure 11a,b show the comparison between the expected theoretical value and the tracked maximum power point, obtained by simulation and experimentation, while Table 6 summarizes the tracking efficiency η of both methods, calculated in accordance with:

$$\eta = \frac{\sum_{n=1}^{m} \frac{P_n}{m}}{P_{ref}} \cdot 100\%. \quad (13)$$

where P_{ref} is the expected theoretical value, m is the number of samples counted in each irradiance level, and P_n is the power at the nth sample.

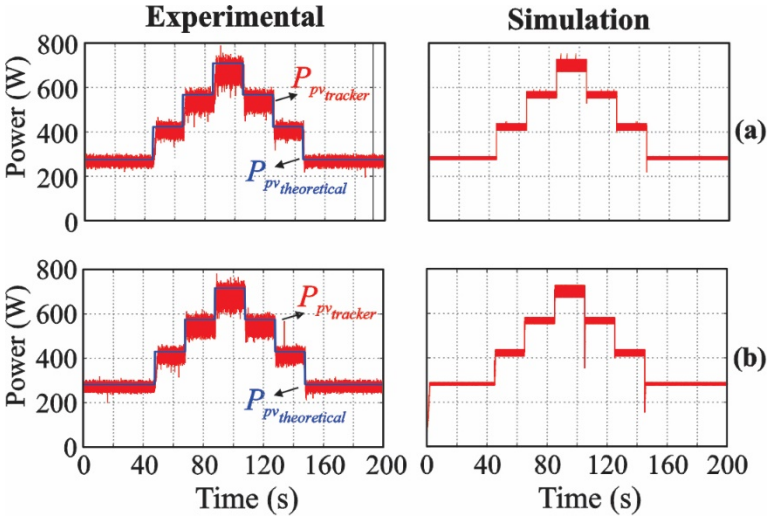

Figure 11. Experimental and simulated results regarding the PV array output power under irradiance changes: (**a**) current sensorless proposed algorithm; (**b**) classical IncCond algorithm.

Table 6. Comparison between the proposed and the classical IncCond algorithms under steps of irradiance.

T [°C]	S [W/m^2]	P_{ref} [W]	Classical IncCond		Proposed IncCond	
			P_{pv} [W]	η [%]	Power [W]	η [%]
47	1000	717	674	94.0	669	93.7
	800	575	542	94.2	537	93.8
	600	430	410	95.4	408	94.9
	400	284	271	95.5	270	95.1

Furthermore, tests were performed by maintaining the irradiance and the load resistance constants at 1000 W/m^2 and 94.4 Ω, respectively. The temperature profile was set to evolve on every 20 s accordingly to the following values: 25 °C, 47 °C and 70 °C. Figure 12a,b depicts simulation and experimental results under the mentioned condition for both methods, while Table 7 summarizes the tracking efficiency η of both methods.

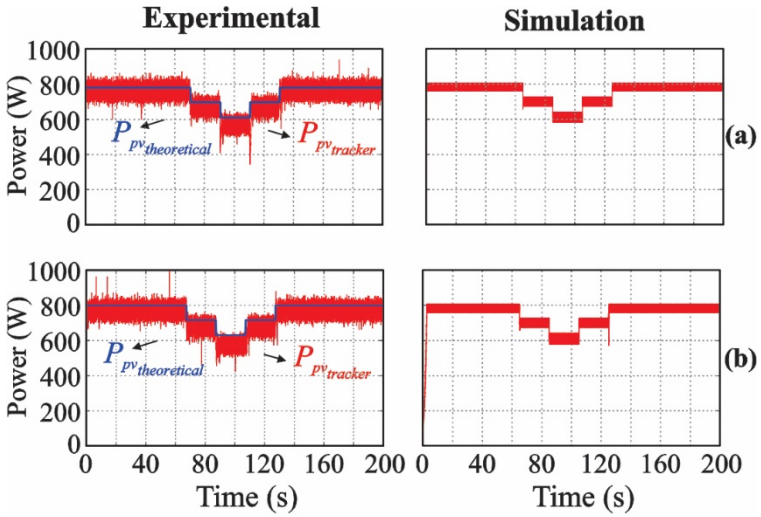

Figure 12. Experimental and simulated results regarding the PV array output power under temperature changes: (**a**) current sensorless proposed algorithm; (**b**) classical IncCond algorithm.

Table 7. Comparison between the proposed and the classical IncCond algorithms under steps of temperature.

T [°C]	S [W/m^2]	P_{ref} [W]	Classical IncCond		Proposed IncCond	
			P_{pv} [W]	η [%]	Power [W]	η [%]
25	1000	800	770	96.3	764	95.5
47	1000	717	674	94.0	669	93.3
70	1000	631	573	90.7	573	90.8

In Figures 11 and 12, it is also possible to note that measured PV output powers are many times greater than the theoretical ones for both methods. However, it is important to highlight that this is impossible to occur. The tracking power will always be lower than the available power in any condition. This just happened because the measured powers have been acquired using the math channel of the oscilloscope, by multiplying the current and voltage measurements, which were subjected to noise. The usage of low-pass filters would fix the problem, but it was decided to present the results without any extra treatment.

As can be observed from the experimental and simulated results, after the transient response, the tracked power matches the expected theoretical value. The performance of the proposed method is very close to the classical one when figures of merit like response

time, steady-state oscillation around the MPP and tracking efficiency are considered. Additionally, the experimental results show that the proposed method presented an average efficiency of 94.0%, a value near to the average efficiency obtained by the classical IncCond method, established at 94.3%.

Additionally, in a broader analysis, Table 8 compares the main features of the proposed algorithm in respect with other methods previously published in the literature, including the perturb and observe (P&O) [43,44], fuzzy logic controller (FLC) [43,44], artificial neural network (ANN) [43], sliding mode (SM) [45], synergetic controller (SC) [45], voltage oriented (VO) [46], and current oriented (CO) [46] MPPT algorithms.

Table 8. Comparison between the proposed algorithm with other ones previously published in the literature.

Algorithm	Main Features
SM-MPPT	• simple implementation • needs at least two sensors (voltage and current) • shows chattering phenomenon • uses first order derivative • intermediate performance
SC-MPPT	• more complex implementation when compared to SM-MPPT • need at least two sensors (voltage and current) • does not show the chattering phenomenon. • uses second order derivative • high performance
P&O-MPPT	• well known algorithm • simple implementation • need at least two sensors (voltage and current) • shows oscillation around the operating point • low performance
FLC-MPPT	• more complex implementation when compared to SM-MPPT • need at least two sensors (voltage and current) • presents less oscillation around the operating point when compared to the P&O • intermediate performance
ANN-MPPT	• performance depends on the network characteristics and number of monitored variables • not intuitive implementation • superior performance when compared to the P&O and FC
VO-MPPT	• well known technique • simple implementation • usually associated with current control to prevent loss of control during fast irradiance changes
CO-MPPT	• well known technique • simple implementation • may present loss of control during sudden changes in irradiance
Proposed	• simple implementation • performance similar to the classical incremental conductance method • use only one voltage sensor • intermediate performance

The comparative analysis of the metrics described for each method in Table 8 allows verifying the proposed method is advantageous in terms of simplicity of implementation and number of sensors, making it a low cost MPPT algorithm. As the desired performance is higher, methods based on artificial intelligence may become more useful. However, the complexity of implementation and the need for computational capacity are greater.

In this context, it is worth mentioning that the proposed algorithm does not compete with the listed algorithm but appears as a proper candidate to substitute the classical

incremental conductance algorithm, since both have similar tracking factors and dynamics behaviors, whereas only the proposed algorithm requires a single voltage sensor.

6. Conclusions

A novel maximum power point tracking method was proposed in this paper. This new algorithm is a modified version of the traditional incremental conductance method, in which the current sensor is suppressed and only a single voltage sensor is required. Several profiles of solar irradiance and temperature were considered for a proper experimental evaluation of the proposed algorithm. As a result, it is concluded that the proposed method is featured by the same advantages of the traditional InCond method, reaching an average tracking factor of about 94%. The main disadvantage of the proposed method is the fact that, in its current form, it cannot be employed in grid-tie single-stage inverters. For its implementation, some modifications are required and, hence, may be evaluated in future works.

Author Contributions: Conceptualization, J.W.Z., W.M.S., D.C.M. and R.F.C.; Methodology, J.W.Z. and R.F.C.; Formal analysis, V.F.G., W.M.S., T.A.P., L.S. and R.F.C.; Investigation, J.W.Z. and T.A.P.; Writing—original draft, V.F.G. and R.F.C.; Writing—review & editing, L.S. and D.C.M.; Funding acquisition, R.F.C. All authors have read and agreed to the published version of the manuscript.

Funding: This research was funded by National Council for Scientific and Technological Development—Process number: 316053/2021-0 and by Graduate Program in Electrical Engineering (PPGEEL)—CAPES/PROEX—Code number: 41001010005P1.

Institutional Review Board Statement: Not applicable.

Informed Consent Statement: Not applicable.

Data Availability Statement: Not applicable.

Conflicts of Interest: The authors have no conflict of interest to declare.

References

1. Good, C.; Andresen, I.; Hestnes, A.G. Solar energy for net zero energy buildings—A comparison between solar thermal, PV and photovoltaic–thermal (PV/T) systems. *Solar Energy* **2015**, *122*, 986–996. [CrossRef]
2. Fraunhofer Institute for Solar Energy Systems, ISE. *Photovoltaics Report*; Fraunhofer Institute for Solar Energy Systems, ISE: Freiburg, Germany, 2022.
3. Spagnuolo, G.; Franco, E.; Bastidas-Rodriguez, J.D.; Ramos-Paja, C.A.; Petrone, G. Maximum power point tracking architectures for photovoltaic systems in mismatching conditions: A review. *IET Power Electron.* **2014**, *7*, 1396–1413. [CrossRef]
4. Subudh, B.; Pradhan, R. A Comparative study on maximum power point tracking techniques for photovoltaic power systems. *IEEE Trans. Sustain. Energy* **2013**, *4*, 89–98. [CrossRef]
5. Mastromauro, R.A.; Liserre, M.; Dell'Aquila, A. Control issues in single-stage photovoltaic systems: MPPT, current and voltage control. *IEEE Trans. Ind. Inform.* **2012**, *8*, 241–254. [CrossRef]
6. Esram, T.; Chapman, P.L. Comparison of photovoltaic array maximum power point tracking techniques. *IEEE Trans. Energy Convers.* **2007**, *22*, 439–449. [CrossRef]
7. Devarakonda, A.K.; Karuppiah, N.; Selvaraj, T.; Balachandran, P.K.; Shanmugasundaram, R.; Senjyu, T. A comparative analysis of maximum power point techniques for solar photovoltaic systems. *Energies* **2022**, *15*, 8776. [CrossRef]
8. Rezk, H.; Eltamaly, A.M. A comprehensive comparison of different MPPT techniques for photovoltaic systems. *Solar Energy* **2015**, *112*, 1–11. [CrossRef]
9. Derbeli, M.; Napole, C.; Barambones, O.; Sanchez, J.; Calvo, I.; Fernández-Bustamante, P. Maximum power point tracking techniques for photovoltaic panel: A review and experimental applications. *Energies* **2021**, *14*, 7806. [CrossRef]
10. Coelho, R.F.; Concer, F.M.; Martins, D.C. Analytical and experimental analysis of DC-DC converters in photovoltaic maximum power point tracking applications. In Proceedings of the IECON 2010-36th Annual Conference on IEEE Industrial Electronics Society, Glendale, GA, USA, 7–10 November 2010; pp. 2778–2783. [CrossRef]
11. Enrique, J.M.; Durán, E.; Sidrach-de-Cardona, M.; Andújar, J.M. Theoretical assessment of the maximum power point tracking efficiency of photovoltaic facilities with different converter topologies. *Solar Energy* **2007**, *81*, 31–38. [CrossRef]
12. Coelho, R.F.; dos Santos, W.M.; Martins, D.C. Influence of power converters on PV maximum power point tracking efficiency. In Proceedings of the 2012 10th IEEE/IAS International Conference on Industry Applications, Fortaleza, Brazil, 5–7 November 2012; pp. 1–8. [CrossRef]

13. Coelho, R.F.; Concer, F.M.; Martins, D.C. A simplified analysis of DC-DC converter applied as maximum power point tracker in photovoltaic systems. In Proceedings of the 2nd International Symposium on Power Electronics for Distributed Generation Systems, Hefei, China, 16–18 June 2010; pp. 29–34. [CrossRef]
14. Seguel, J.L.; Seleme, S.I., Jr.; Morais, L.M.F. Comparative study of Buck-Boost, SEPIC, Cuk and Zeta DC-DC converters using different MPPT methods for photovoltaic applications. *Energies* **2022**, *15*, 7936. [CrossRef]
15. Mishra, S.; Sekhar, P.C. Takagi–Sugeno fuzzy-based incremental conductance algorithm for maximum power point tracking of a photovoltaic generating system. *IET Renew. Power Gener.* **2014**, *8*, 900–914. [CrossRef]
16. Elobaid, L.M.; Abdelsalam, A.K.; Zakzouk, E.E. Artificial neural network-based photovoltaic maximum power point tracking techniques: A survey. *IET Renew. Power Gener.* **2015**, *9*, 1043–1063. [CrossRef]
17. Li, X.; Wen, H.; Jiang, L.; Hu, Y.; Zhao, C. An improved beta method with autoscaling factor for photovoltaic system. *IEEE Trans. Ind. Appl.* **2016**, *52*, 4281–4291. [CrossRef]
18. Li, X.; Wen, H.; Hu, Y.; Jiang, L.; Xiao, W. Modified beta algorithm for GMPPT and partial shading detection in photovoltaic systems. *IEEE Trans. Power Electron.* **2018**, *33*, 2172–2186. [CrossRef]
19. Sera, D.; Mathe, L.; Kerekes, T.; Spataru, S.V.; Teodorescu, R. On the perturb-and-observe and incremental conductance MPPT methods for PV systems. *IEEE J. Photovolt.* **2013**, *3*, 1070–1078. [CrossRef]
20. Villalva, M.G.; Ruppert, F.E. Analysis and simulation of the P&O MPPT algorithm using a linearized PV array model. In Proceedings of the 2009 35th Annual Conference of IEEE Industrial Electronics, Porto, Portugal, 3–5 November 2009; pp. 231–236. [CrossRef]
21. Femia, N.; Fortunato, M.; Lisi, G.; Petrone, G.; Spagnuolo, G.; Vitelli, M. Guidelines for the optimization of the P&O technique in grid-connected double-stage photovoltaic systems. In Proceedings of the 2007 IEEE International Symposium on Industrial Electronics, Vigo, Spain, 4–7 June 2007. [CrossRef]
22. Femia, N.; Petrone, G.; Spagnuolo, G.; Vitelli, M. Optimization of perturb and observe maximum power point tracking method. *IEEE Trans. Power Electron.* **2005**, *20*, 963–973. [CrossRef]
23. Liu, F.; Duan, S.; Liu, B.; Kang, Y. A variable step size INC MPPT method for PV systems. *IEEE Trans. Ind. Electron.* **2008**, *55*, 622–628. [CrossRef]
24. Williams, B.W.; Helal, A.A.; Elsaharty, M.A.; Abdelsalam, A.K.; Zakzouk, N.E. Improved performance low-cost incremental conductance PV MPPT technique. *IET Renew. Power Gener.* **2016**, *10*, 561–574. [CrossRef]
25. Thangavelu, A.; Vairakannu, S.; Parvathyshankar, D. Linear open circuit voltage-variable step-size-incremental conductance strategy-based hybrid MPPT controller for remote power applications. *IET Power Electron.* **2017**, *10*, 1363–1376. [CrossRef]
26. Huynh, D.C.; Dunnigan, M.W. Development and comparison of an improved incremental conductance algorithm for tracking the MPP of a solar PV panel. *IEEE Trans. Sust. Energy* **2016**, *7*, 1421–1429. [CrossRef]
27. Elgendy, M.A.; Atkinson, D.J.; Zahawi, B. Experimental investigation of the incremental conductance maximum power point tracking algorithm at high perturbation rates. *IET Renew. Power Gener.* **2016**, *10*, 133–139. [CrossRef]
28. Tey, K.S.; Mekhilef, S. Modified incremental conductance algorithm for photovoltaic system under partial shading conditions and load variation. *IEEE Trans. Ind. Electron.* **2014**, *61*, 5384–5385. [CrossRef]
29. Lasheen, M.; Rahman, A.K.A.; Abdel-Salam, M.; Ookawara, S. Adaptive reference voltage-based MPPT technique for PV applications. *IET Renew. Power Gener.* **2017**, *11*, 715–722. [CrossRef]
30. Li, S.; Liao, H.; Yuan, H.; Ai, Q.; Chen, K. A MPPT strategy with variable weather parameters through analyzing the effect of the DC/DC converter to the MPP of PV system. *Solar Energy* **2017**, *144*, 175–184. [CrossRef]
31. Obeidi, N.; Kermadi, M.; Belmadani, B.; Allag, A.; Achour, L.; Mekhilef, S. A current sensorless control of buck-boost converter for maximum power point tracking in photovoltaic applications. *Energies* **2022**, *15*, 7811. [CrossRef]
32. Hussein, K.H.; Muta, I.; Hoshino, T.; Osakada, M. Maximum photovoltaic power tracking: An algorithm for rapidly changing atmospheric conditions. *IEE Proc.-Gener. Transm. Distrib.* **1995**, *142*, 59–64. [CrossRef]
33. Ho, B.M.T.; Chung, H.S.H.; Lo, W.L. Use of system oscillation to locate the MPP of PV panels. *IEEE Power Electron. Lett.* **2004**, *2*, 1–5. [CrossRef]
34. Karbakhsh, F.; Amiri, M.; Abootorabi, Z.H. Two-switch flyback inverter employing a current sensorless MPPT and scalar control for low-cost solar powered pumps. *IET Renew. Power Gener.* **2017**, *11*, 669–677. [CrossRef]
35. Abbassi, A.; Gammoudi, R.; Dami, A.M.; Hasnaoui, O.; Jemli, M. An improved single-diode model parameters extraction at different operating conditions with a view to modeling a photovoltaic generator: A comparative study. *Solar Energy* **2017**, *155*, 478–489. [CrossRef]
36. Yeh, W.C.; Lin, P.; Huang, C.L. Simplified swarm optimisation for the solar cell models parameter estimation problem. *IET Renew. Power Gener.* **2017**, *11*, 1166–1173. [CrossRef]
37. Batzelis, E.I.; Papathanassiou, S.A. A method for the analytical extraction of the single-diode PV model parameters. *IEEE Trans. Sustain. Energy* **2016**, *7*, 504–512. [CrossRef]
38. Seddaoui, N.; Rahmani, L.; Chauder, A.; Kessal, A. Parameters extraction of photovoltaic module at reference and real conditions. In Proceedings of the 2011 46th International Universities' Power Engineering Conference (UPEC), Soest, Germany, 5–8 September 2011.
39. Lappalainen, K.; Valkealahti, S. Effects of irradiance transition characteristics on the mismatch losses of different electrical PV array configurations. *IET Renew. Power Gener.* **2017**, *11*, 248–254. [CrossRef]

40. Hejri, M.; Mokhtari, H.; Azizian, M.R.; Ghandhari, M.; Soder, L. On the parameter extraction of a five-parameter double-diode model of photovoltaic cells and modules. *IEEE J. Photovolt.* **2014**, *4*, 915–923. [CrossRef]
41. Teodorescu, R.; Liserre, M.; Rodríguez, P. *Grid Converters for Photovoltaic and Wind Power Systems*, 1st ed.; John Wiley & Sons: Chicheter, UK, 2011; pp. 289–312.
42. Baba, A.O.; Liu, G.; Chen, X. Classification and Evaluation Review of Maximum Power Point Tracking Methods. *Sustain. Futures* **2020**, *2*, 100020. [CrossRef]
43. Kumar, N.; Dahiya, A.K. Implementation and Comparison of Perturb & Observe, ANN and ANFIS Based MPPT Techniques. In Proceedings of the 2018 International Conference on Inventive Research in Computing Applications (ICIRCA), Coimbatore, India, 11–12 July 2018; pp. 1–5. [CrossRef]
44. Belgacem, A.M.; Hadef, M.; Djerdir, A. Comparative Study MPPT between FLC and Incremental Conductance Applied on PV Water Pumping System. In Proceedings of the 2022 19th International Multi-Conference on Systems, Signals & Devices (SSD), Sétif, Algeria, 6–10 May 2022; pp. 1394–1400. [CrossRef]
45. Ayat, R.; Bouafia, A.; Gaubert, J.-P. Experimental validation of synergetic approach based MPPT controller for an autonomous PV system. *IET Renew Power Gener.* **2021**, *15*, 1515–1527. [CrossRef]
46. Raiker, G.A.; Loganathan, U.; Reddy, B.S. Current Control of Boost Converter for PV Interface With Momentum-Based Perturb and Observe MPPT. *IEEE Trans. Ind. Appl.* **2021**, *4*, 4071–4079. [CrossRef]